# Potential Flow Over Bodies of Revolution in Unsteady Motion

Ming-Shin Wu,* Pablo Garcia-Fogeda,† and D. D. Liu‡
*Arizona State University, Tempe, Arizona*

**The problem of axisymmetric bodies performing rigid and bending oscillations in an incompressible flow has been investigated. A line source/doublet element method has been developed for computation of pressures, forces, and moments for bodies in steady and oscillatory motion. A new "$\mu - \sigma$ rule" is derived to relate the dipole strength to the local body geometry in the crossflow instead of extending the commonly used "inset distance" method. The bodies under consideration are required to be smooth in curvature and have closed ends. The method is otherwise general in body geometries, reduced frequencies, and mode shapes of oscillations. In the case of steady flow, good agreement is found with the results of Hess's surface panel method and Lamb's exact solution. For bodies in rigid oscillations, studies were carried out to investigate the effects of the body thickness and nose curvature on the unsteady pressures and stability derivatives. It is found that bodies with blunt noses are statically unstable and dynamically stable whereas those with sharp noses are statically and dynamically unstable. For elastic bodies in bending oscillations, unsteady pressures and local damping forces are obtained, including body thickness effects at high reduced frequencies. In all cases considered, the present results approach the slender-body-theory limit in a consistent manner.**

## Nomenclature

| | |
|---|---|
| $C_{p0}$ | = mean pressure coefficient |
| $\hat{C}_p$ | = unsteady pressure coefficient |
| $g(x)$ | = normalized natural mode shape |
| $k$ | = $\omega L / U_\infty$, reduced frequency |
| $L$ | = body length |
| $R$ | = $R(x)$, the body surface |
| $U_\infty$ | = freestream velocity |
| $x, r, \theta$ | = nondimensional cylindrical coordinates |
| $x_G$ | = center of oscillation |
| $t$ | = nondimensional time |
| $\delta_0$ | = amplitude of oscillation |
| $\epsilon$ | = inset distance |
| $\mu$ | = exponent of the dipole strength for the irregular panels |
| $\xi$ | = source or dipole coordinate |
| $\sigma$ | = exponent of the body shape at the apex |
| $\tau$ | = body thickness ratio |
| $\phi_0$ | = axial-flow perturbation potential |
| $\phi_1$ | = unsteady flow perturbation potential |
| $\omega$ | = circular frequency |
| $\Omega$ | = full velocity potential |

## Introduction

MANY vehicles traveling in air or in the ocean have axisymmetric shapes. These include airships, drones, stores, and fuel tanks for low-speed aircraft, submarines, and torpedos. In practice, engineers are interested in predicting aerodynamic or hydrodynamic loads accurately on these bodies for vehicle control, performance, and design. Classical methods of studying these problems are based on the slender-body approach. Although slender-body solutions (e.g., Refs. 1 and 2) provide the basis for other improved solutions, they have two basic limitations. They do not include thickness effects and are only valid in the proximity of the body. In practice, the slender-body theory alone would not be satisfactory for predictions of the lifting forces and moments.

In order to account for the full problem, two basic issues must be addressed. These are the effects due to body geometry, thickness, and body motion and those due to the body wake. The latter has been an open issue related to unresolved questions of flow separation and wake modeling. In the present analysis, we therefore exclude the consideration of wake modeling and focus on the former issue in body effects. To account for the full thickness effect, the common approach is to start from an inviscid potential flow formulation for a steady or unsteady problem.

During the 1930's, von Kármán[3] first introduced the line-source element method using the stream function as the dependent variable. Oberkampf and Watson[4] studied the method more extensively and found that, in general, the linear system of equations produced by this method is ill-conditioned. Later, Zedan and Dalton[5] employed a mixed linear-quadratic line-source distribution along the body axis and showed some success for bodies of revolution at zero angle of attack. However, since the stream function approach is limited to two-dimensional (or axisymmetric) flows, other investigators used the velocity potential as the dependent variable. Among them, Kuhlman and Shu[6] claimed success for steady flow employing the line-source method. They found correct inset distances as a function of thickness ratios and that, for the mean flow, the linear line-source distribution is an optimum one that gives the lowest root mean square error.

Hess and Smith[7] first introduced the surface-source panel method. Their subsequent work has demonstrated that their method is robust and versatile in three-dimensional flow applications. Woodward[8] extended their method to linearized subsonic/supersonic Mach numbers (USSAERO Code). These surface-source panel methods have the drawback that for three-dimensional configurations too many panel elements are needed. During the course of the present investigation, it also was found that the USSAERO Code becomes unreliable as the body thickness ratio decreases and does not approach the slender-body limit correctly.

The objective of the present study is to develop an efficient method for the computation of incompressible inviscid irrotational flow past rigid or elastic bodies in oscillation. Such a development results in a computer code for calculations of the unsteady pressures, lifting forces and moments, and stability

Received July 29, 1987; revision received July 21, 1988. 

*Graduate Student, Department of Mechanical and Aerospace Engineering.

†Faculty Associate, Department of Mechanical and Aerospace Engineering; currently Assistant Professor, E.T.S.I. Aeronautics, Madrid, Spain. Member AIAA.

‡Associate Professor, Department of Mechanical and Aerospace Engineering. Member AIAA.

derivatives. In view of the drawbacks of the surface-source panel method, the line-source and line-doublet element (LSDE) methods were adopted for a convenient treatment of bodies in oscillatory motion. Since the steady mean flow enters the unsteady flow formulation through the tangency condition and the unsteady pressure coefficients, it becomes equally important to re-examine the steady panel methods. For the crossflow, a new "$\mu - \sigma$ rule" introduced to model the doublet strength function, i.e., $m(\xi) = a\xi^{\mu} + b\xi + c$. It is found that the exponent $\mu$ can be best determined in the range from $\mu = 2$ to $\mu > 2$, depending on the body nose curvature at the edge panels (irregular panels) for all given body shapes. In the present study, only bodies with smooth body slope and closed ends are presented.

## Analysis

### Coordinate System

For bodies in rigid oscillation, a body-fixed coordinate system is employed. This system requires that the $x$ axis remain at all times the axis of the body, whereby each right cross section is circular and contains the $r$ axis (see Fig. 1). Following Revell,[9,10] the nondimensional full velocity potential $\Omega$ for a body of revolution can be expressed in this system as

$$\Omega(x,r,\theta,t) = x + \delta(t)r\cos\theta + \phi_0(x,r) + \delta(t)\phi_1(x,r)\cos\theta \quad (1)$$

where $\Omega$, $\phi_0$, and $\phi_1$ are nondimensional potentials that have been normalized by $U_\infty L$; $U_\infty$ is the freestream velocity and $L$ the body length. Independent variables $(x,r)$ and $t$ are the nondimensional coordinates and time, which are normalized by $L$ and $L/U_\infty$, respectively, and $\phi_0$ is the mean flow potential, $\phi_1$ the unsteady flow potential, and $\delta(t)$ the instantaneous amplitude of oscillation. For harmonic motions, $\delta(t)$ can be written as $\delta(t) = \delta_0 e^{ikt}$, where $\delta_0$ is the amplitude of oscillation and $k$ the reduced frequency.

The total velocity then can be obtained as

$$\begin{aligned}\nabla\Omega = {} & [1 + \phi_{0_x} + \delta(t)\phi_{1_x}\cos\theta]e_x \\ & + [\phi_{0_r} + \delta(t)\phi_{1_r}\cos\theta + \delta(t)\cos\theta]e_r \\ & - \delta(t)[\sin\theta + (1/r)\phi_1\sin\theta]e_\theta \end{aligned} \quad (2)$$

Substituting Eq. (2) into the continuity equation and collecting terms of like order yields the unified governing equations for $\phi_0$ and $\phi_1$, which are the Laplace equations

$$\phi_{\lambda_{xx}} + \phi_{\lambda_{rr}} + (1/r)\phi_{\lambda_r} - (\lambda/r^2)\,\phi_\lambda = 0 \quad (3)$$

where $\lambda = 0$ for $\phi_0$ and $\lambda = 1$ for $\phi_1$. Both $\phi$ are independent of $\theta$.

### Method of Solution

The integral solutions of Eq. (3) are

$$\phi_\lambda(x,r) = \int_{\epsilon}^{1-\epsilon} f_\lambda(\xi)\cdot K_\lambda(x-\xi,r)\,d\xi \quad (4)$$

where $f_0(\xi)$ and $f_1(\xi)$ represent the source and doublet strength functions, respectively. The associated kernel functions are

$$K_0 = \frac{1}{\sqrt{(x-\xi)^2 + r^2}} \quad (5)$$

$$K_1 = \frac{r}{\sqrt{[(x-\xi)^2 + r^2]^3}} \quad (6)$$

and $\epsilon$ is the inset distance imposed at both ends of the body (see Fig. 2, where $\epsilon = \xi_1$ or $1 - \xi_{N+1}$).

In the limit of $\epsilon$ approaching zero, Eq. (4) is a Fredholm integral equation of the first kind. Pichard[11] has given various conditions under which he proves that certain exact solutions

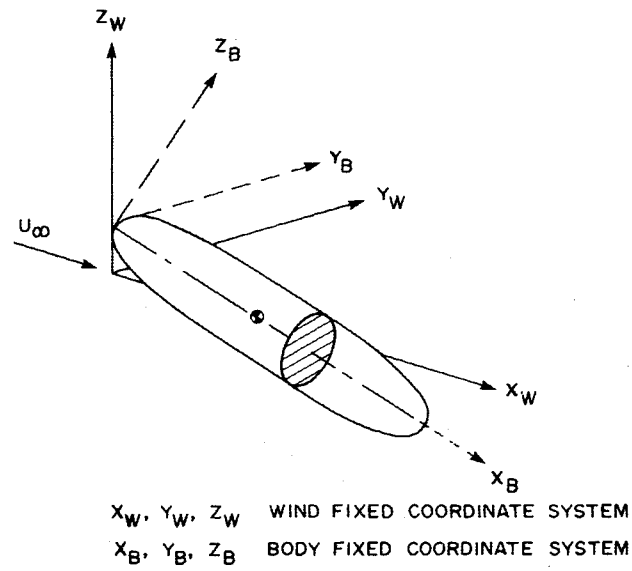


**Fig. 1 Wind-fixed and body-fixed coordinate systems for an oscillating rigid body.**

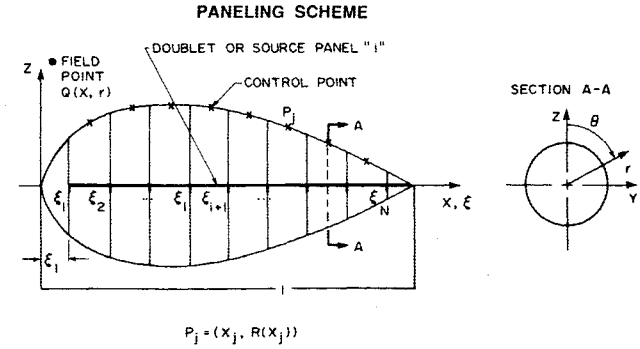


**Fig. 2 Element arrangements for axisymmetric bodies.**

of this type of equation do exist. Landweber[12] subsequently has obtained an iteration formula with which the solution is proved to coverge through the proposed successive approximation procedure. The problem that arises in these methods is that the procedures appear to be tedious and restrictive for practical applications. Based on the Munk-Jones's slender-body solution,[1,13] Adams and Sears[14] have developed an iterative series expansion method to solve the same integral equation for not-so-slender bodies in compressible flow. Yet their solutions are only valid in the near field.

In contrast to these approaches, we have developed a line source/doublet element (LSDE) method to solve Eq. (4) numerically for arbitrary bodies in unsteady motion. According to the LSDE method, Eq. (4) is first discretized as

$$\phi_\lambda(x_j,r_j) = \sum_{i=1}^{N}\int_{\xi_i}^{\xi_{i+1}} f_{\lambda_i}(\xi)\cdot K_\lambda(x_j-\xi,r_j)\,d\xi \quad (7)$$

where

$$\begin{aligned} f_{0i}(\xi) &= a_{0i}\xi + b_{0i} \\ f_{1i}(\xi) &= a_{1i}\xi^{\mu} + b_{1i}\xi + c_{1i} \end{aligned} \quad (8)$$

and $N$ is the total number of elements.

During the course of our studies, we found that the use of one type of element with a fixed doublet strength exponent [e.g., $\mu = 2$ for $f_{11}(x)$] for the crossflow results in an inaccurate local numerical solution at both ends of the body. Thus, two different types of elements are categorized in our formulation. The leading- and trailing-edge elements are defined as irregu-

lar elements where the value of $\mu$ is related to the local body geometry, and the rest are regular elements where $\mu$ is set to two.

To relate $\mu$ to the local geometry, an asymptotic analysis of the integral solution at the body end points is carried out. For the leading-edge panel, the velocities in the $x$ and $r$ directions can be expressed as

$$\phi_{1x} = f_{11}(x)\int_0^p \frac{\partial K_1}{\partial x}\,d\xi + f'_{11}(x)\int_0^p (\xi - x)\frac{\partial K_1}{\partial x}\,d\xi + f''_{11}(x)\int_0^p \frac{(\xi-x)^2}{2}\frac{\partial K_1}{\partial x}\,d\xi + \ldots \tag{9}$$

$$\phi_{1r} = f_{11}(x)\int_0^p \frac{\partial K_1}{\partial r}\,d\xi + f'_{11}(x)\int_0^p (\xi - x)\frac{\partial K_1}{\partial r}\,d\xi + f''_{11}(x)\int_0^p \frac{(\xi-x)^2}{2}\frac{\partial K_1}{\partial r}\,d\xi + \ldots \tag{10}$$

where $p$ is the length of the leading-edge element. Upon intergration, Eqs. (9) and (10) can be recast into

$$\phi_{1x} \simeq f_{11}(x)Q_0(x,p,r) + f'_{11}(x)Q_1(x,p,r) + f''_{11}(x)Q_2(x,p,r) + \ldots \tag{11}$$

$$\phi_{1r} \simeq f_{11}(x)S_0(x,p,r) + f'_{11}(x)S_1(x,p,r) + f''_{11}(x)S_2(x,p,r) + \ldots \tag{12}$$

where the functions $Q_i$ and $S_i$ are known functions of $x$, $p$, and $r$ describing the flowfield influence on this element.

Now, if the body shape at the apex is assumed in the form of $R(x) = Cx^\sigma$, where $C$ and $\sigma$ are positive real numbers, the normal velocity on the body surface can be expressed as

$$\frac{\partial \phi_1}{\partial n} = \phi_{1r}(x, Cx^\sigma) - C\sigma x^{\sigma-1}\phi_{1x}(x, Cx^\sigma) \tag{13}$$

When Eq. (13) is combined with Eqs. (11) and (12) and $f_{11}(x)$ is set to $a_{11}x^\mu$, the normal velocity $\partial\phi_1/\partial n$ can be expanded for small $x$ to yield the asymptotic series

$$\frac{\partial \phi_1}{\partial n} = A_1 x^{\mu-3\sigma+1} + A_2 x^{\mu-\sigma-1} + A_3 x^{\mu-2}\ln x + A_4 x^{\mu-3+\sigma} + \ldots \qquad \text{for } \sigma < 1 \text{ (blunt nose)} \tag{14}$$

or

$$\frac{\partial \phi_1}{\partial n} = A_5 x^{\mu-2\sigma} + A_6 x^{\mu-2} + A_7 x^{\mu-4+2\sigma} + A_8 x^{\mu+4\sigma-6} + \ldots \qquad \text{for } \sigma \geq 1 \text{ (sharp nose)} \tag{15}$$

where the $A_i$ are constants that depend on the values of $C$ and $p$.

To relate $\mu$ to $\sigma$, we impose the finiteness condition for $\partial\phi/\partial n$ at the body apex. Thus, we obtain

$$\mu = 3 - \sigma \qquad \text{for } \sigma < 1$$

$$\mu = 2\sigma \qquad \text{for } \sigma \geq 1 \tag{16}$$

This is defined as the "$\mu - \sigma$ rule." The same results can be obtained if this asymptotic analysis is carried out at the trailing edge. It should be noted that Eq. (16) does not generally serve as the exact $\mu - \sigma$ relation in that the $\mu$ value will slightly increase if more terms in the series are included in the analysis. However, for sharp-nose bodies, our investigation shows that $\mu = 2\sigma$ remains unchanged for $\sigma \geq 2$ when the series is truncated up to the sixth term. In any case, the three-term expansion result obtained in Eq. (16) is considered sufficient for the determination of $\mu$. By sufficient, it is meant that the $\mu - \sigma$ rule here will serve as a lower bound for $\mu$ in order to ensure the finiteness of the crossflow solution at the body edges. It should be pointed out that the $\mu - \sigma$ rule is more general than Moran's inset-distance approach. The reasons are the following:

1) The $\mu - \sigma$ rule is a direct approach in that it provides the specific singularity strength $\mu$ on the irregular elements considered, whereas the inset-distance approach only provides a distance $\epsilon$ from the apex, which is not pertinent to the present LSDE method.

2) The $\mu - \sigma$ rule is developed for crossflow problems here, steady or unsteady, while the inset-distance technique was developed for axial flow only. The $\mu - \sigma$ rule can be generalized to bodies with local concave or convex corners for both axial and crossflow problems.

Applying the condition of continuous source/dipole strength between panels and differentiating Eq. (7) with respect to $x$ and $r$, we obtain

$$\phi_\lambda(x_j, r_j) = \sum_{i=1}^{N} (a_\lambda)_i\,(A_\lambda)_{ij} \tag{17}$$

$$\phi_{\lambda_x}(x_j, r_j) = \sum_{i=1}^{N} (a_\lambda)_i\,(B_\lambda)_{ij} \tag{18}$$

$$\phi_{\lambda_r}(x_j, r_j) = \sum_{i=1}^{N} (a_\lambda)_i\,(C_\lambda)_{ij} \tag{19}$$

The unknown source and doublet strengths then can be obtained by satisfying the tangency condition on the body surface,

$$\sum_{i=1}^{N} (a_\lambda)_i\,[(C_\lambda)_{ij} - R'(x_j)(B_\lambda)_{ij}] = R'(x_j), \qquad \text{for } \lambda = 0 \tag{20}$$

$$= -1 - ik[R(x_j)R'(x_j) + x_j - x_G], \qquad \text{for } \lambda = 1 \tag{21}$$

where $j = 1,2,\ldots,N$.

#### Flexible Body Formulation

For flexible bodies in bending oscillation, the wind-fixed system is employed. This system requires that the $x$ axis remain parallel to the freestream velocity at all times. Accordingly, the full velocity potential can be recast into

$$\Omega(x, r, \theta, t) = x + \phi_0(x, r) + \delta(t)\,\phi_1(x, r)\cos\theta \tag{22}$$

where $\phi_0$ and $\phi_1$ satisfy Eq. (3) for $\lambda = 0$ and $\lambda = 1$. Similarly, the unknown strength $(\tilde{a}_\lambda)_i$ can be obtained by solving the wind-fixed tangency conditions (see Ref. 15) on the mean body surface,

$$\sum_{i=1}^{N} (\tilde{a}_\lambda)_i\,[(\tilde{C}_\lambda)_{ij} - (\tilde{B}_\lambda)_{ij}R'(x_j)] = R'(x_j), \qquad \text{for } \lambda = 0 \tag{23}$$

$$= g(x_j)[\phi_{0_{rr}} - R'(x_j)\,\phi_{0_{xr}}(x_j)] - g'(x_j)(1 + \phi_{0_x}) - ikg(x_j), \qquad \text{for } \lambda = 1 \tag{24}$$

where $g(x)$ is the body mode shape.

#### Pressures and Stability Derivatives

The exact isentropic pressure coefficient can be expanded to yield the mean flow and the unsteady flow pressure coefficients. In the body-fixed coordinate system, these pressure coefficients read

$$C_p = C_{p_0} + \delta_0 e^{ikt}\hat{C}_p\cos\theta \qquad \text{at } r = R(x) \tag{25}$$

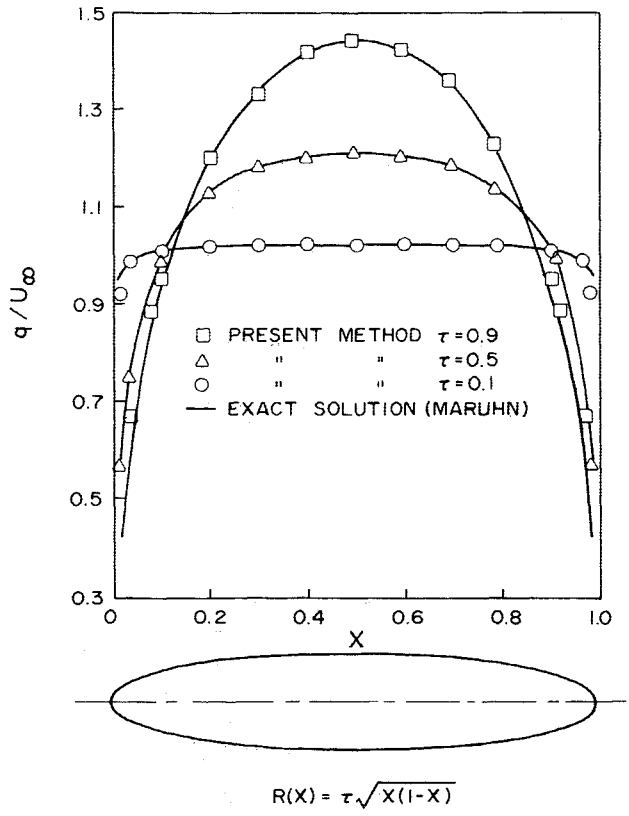


**Fig. 3 Exact and computed velocity distribution for ellipsoid of various thickness ratios ($\alpha$ deg = 0, inset = 0.01).**

where

$$C_{p_0} = -(2\phi_{0_x} + \phi_{0_x}^2 + \phi_{0_r}^2) \tag{26}$$

$$\hat{C}_p = -2[(1+\phi_{0_x})\phi_{1_x} + (1+\phi_{1_r})\phi_{0_r} + ik[\phi_1 - R\phi_{0_x} + (x-x_G)\phi_{0_r}] \tag{27}$$

The unsteady pressure $C_p$ in Eq. (23) is not correctly represented in the wind-fixed coordinate system. To obtain the correct $C_p$, it is required to remove the resulting implicit dependence on $\delta$ in $\phi_0$ and $\phi_1$, as was pointed out by Hoffman and Platzer.[16] Hence, performing a Taylor series expansion on these variables about the mean position yields

$$\hat{C}_p = -2\{-g[(1+\phi_{0_x})\phi_{0_{xr}} + \phi_{0_r}\phi_{0_{rr}}] + (1+\phi_{0_x})\phi_{1_x} + \phi_{0_r}\phi_{1_r} + ik\phi_1\} \qquad \text{at } r = R(x) \tag{28}$$

It should be noted that the unsteady pressure coefficient $C_p$ also can be expressed as

$$\hat{C}_p = C_{p_1} + ikC_{p_2} \tag{29}$$

where $C_{p_1}$ and $C_{p_2}$ are real functions. Finally, the stability derivatives can be expressed in terms of the in-phase and out-of-phase pressure coefficients. For stiffness derivatives,

$$C_{N_\alpha} = \frac{-4}{\tau^2}\int_0^1 RC_{p_1}(x,R)\,dx \tag{30}$$

$$C_{M_\alpha} = \frac{-4}{\tau^2}\int_0^1 (x-x_G)RC_{p_1}(x,R)\,dx \tag{31}$$

For damping derivatives,

$$C_{N_{\dot\alpha}} = \frac{4}{\tau^2}\int_0^1 RC_{p_2}(x,R)\,dx \tag{32}$$

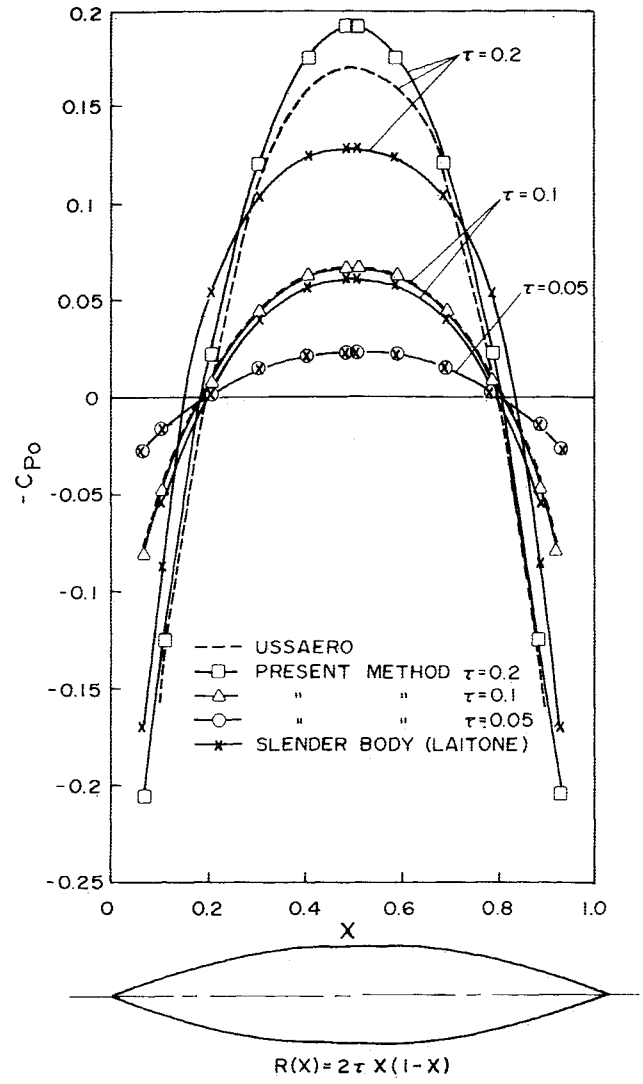


**Fig. 4 Comparison of body surface pressure coefficient for a parabolic spindle at zero angle of attack (inset = 0).**

$$C_{M_{\dot\alpha}} = \frac{4}{\tau^2}\int_0^1 (x-x_G)RC_{p_2}(x,R)\,dx \tag{33}$$

## Results and Discussion

### Mean Flow Results

Mean flow pressures and velocity distributions for various bodies at zero incidence are computed. Figure 3 shows the comparison in the total velocity distribution between the present results and Maruhn's exact theory[17] for an ellipsoid. With only 30 elements, excellent agreement is obtained for thickness ratios ranging from $\tau = 0.1$ to $\tau = 0.9$. Figure 4 compares the present results with those computed by USSAERO[8] and Laitone's slender body theory.[2] It is seen that the present results reduce to those according to Laitone's slender-body theory as the thickness ratio decreases, while the USSAERO code fails to check with the slender-body theory for the lowest thickness ratio. Clearly, the present line-source maintains the correct numerical limit, whereas the surface-panel scheme of USSAERO probably does not possess such a limit. As for the difference between USSAERO and the present method for the case of $\tau = 0.2$, further verification is required. Figure 5 presents the computed pressure distributions for the Landweber body. The present result is in good agreement with Hess and Smith's surface-ring-panel method,[7] whereas Moran's first-order theory[18] and Van Dyke's second-order theory,[19] on the other hand, depart from the present and Hess and Smith's

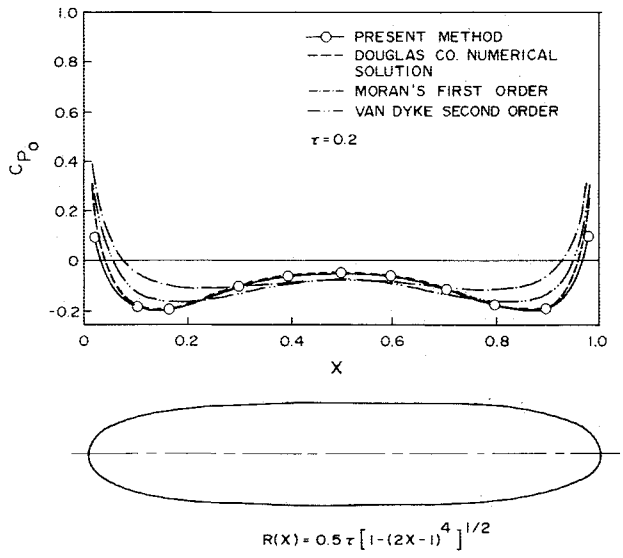


**Fig. 5 Comparison of body surface pressure coefficient for Landweber's body at zero angle of attack ($\tau = 0.2$, inset = 0.0214).**

results at both ends of the body. It would be noted that in all mean flow cases, Moran's rule of inset distance was adopted for computation.

### Inclined Bodies in Steady Flow

Figure 6 shows the comparison of the surface pressure distributions between the present method and Lamb's exact solution[20] for an ellipsoid of thickness ratio $\tau = 0.2$ at an angle of attack $\alpha = 30$ deg. Lamb used the method of Spherical Harmonics to obtain the exact solution of the inclined ellipsoid problem. It is seen that the present results compare very well with Lamb's solution, except in the proximity of the trailing edge.

Figure 7 shows the comparison of the surface pressure distributions between the method, Revell's second-order theory,[9] and Hess and Smith's panel method[7] for a parabolic spindle of thickness ratio $\tau = 0.2$ at an angle of attack $\alpha = 4$ deg. Revell's theory employs the matched asymptotic expansion technique, which provides a second-order approximation to the full potential equation. Hess and Smith's formulation and the present approach are considered to be numerically "exact." It is seen that the present results are in close agreement with those of Hess and Smith and Revell.

### Effects of Body Thickness

Figures 8 and 9 show the effects of thickness ratio on the in-phase and out-of-phase moments for a parabolic spindle pitching about the apex. It is seen that $C_{M_\alpha}$ decreases with increasing thickness ratio, whereas $C_{M_{\dot\delta}}$ is nearly independent of the thickness parameter. However, as the thickness increases further, opposite trends are observed in Fig. 9 between these results.

While the present method and Revell's theory predict a trend of positive damping as the thickness increases, Liu et al.'s theory[21] predicts negative damping. It appears that the latter first-order theory fails to predict the damping derivative correctly beyond certain thickness (around 5% in this case).

### Effects of Nose Curvature

To investigate the influence of nose curvature on the stability derivatives, the body geometry can be described by a generalized formula

$$R(x) = (\tau/2)[4x(1-x)]^\sigma$$

where $\sigma$ defines the shape of the body; $\sigma \geq 1$ for sharp noses and $\sigma < 1$ for blunt noses. These bodies perform pitching oscillations about the body leading edge, i.e., $x_G = 0$.

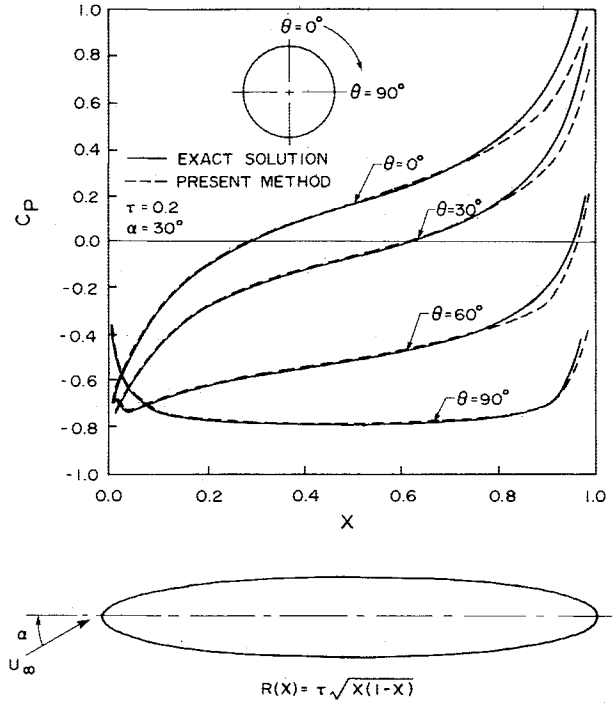


**Fig. 6 Comparison of pressure coefficient for ellipsoid at angle of attack $\alpha = 30$ deg ($\tau = 0.2$).**

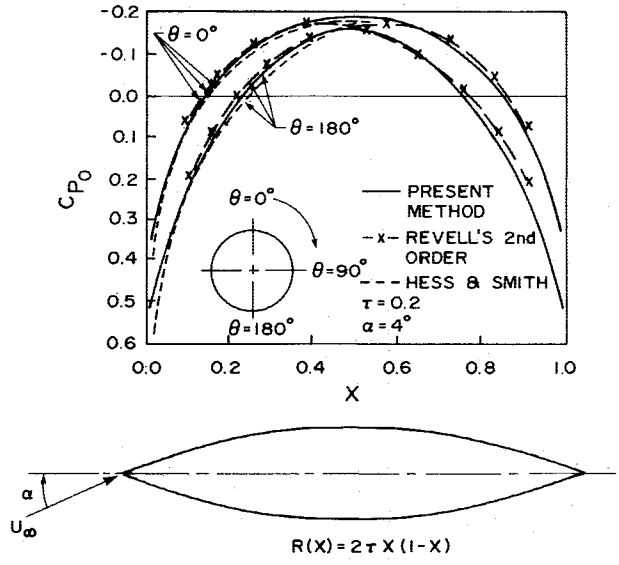


**Fig. 7 Comparison of pressure coefficient for a parabolic spindle at angle of attack $\alpha = 4$ deg ($\tau = 0.2$).**

Figure 10 presents the effect of the nose curvature on the damping-in-pitch normal force coefficient $C_{N_{\dot\delta}}$. As pointed out by Revell,[9] $C_{N_{\dot\delta}}$ represents an "apparent additional mass" opposing the downward acceleration of the body. Therefore, for a fixed thickness ratio $\tau$, $C_{N_{\dot\delta}}$ should decrease as $\sigma$ increases.

In Figs. 11 and 12, the stiffness derivative $C_{M_\alpha}$ and the damping-in-pitch moment coefficient $C_{M_{\dot\delta}}$ are presented for the same family of bodies. It is seen that, whereas $C_{M_\alpha}$ remains positive throughout the range of $\sigma$ considered, $C_{M_{\dot\delta}}$ changes in sign near $\sigma = 0.9$.

The general trends of these stability derivatives can be described in order. Statically, all bodies are unstable, but nose sharpness tends to lessen the static instability. However, dynamically, bodies with blunt noses tend to be more stable; hence, nose sharpness tends to reduce the dynamic stability.

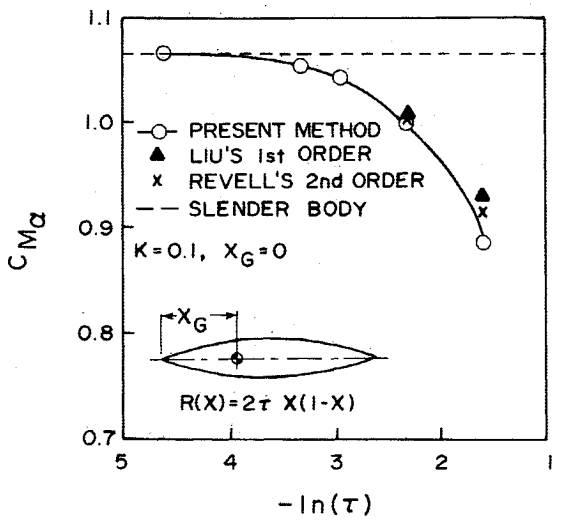


Fig. 8 Effect of thickness ratio on pitching moment coefficient for a parabolic spindle.

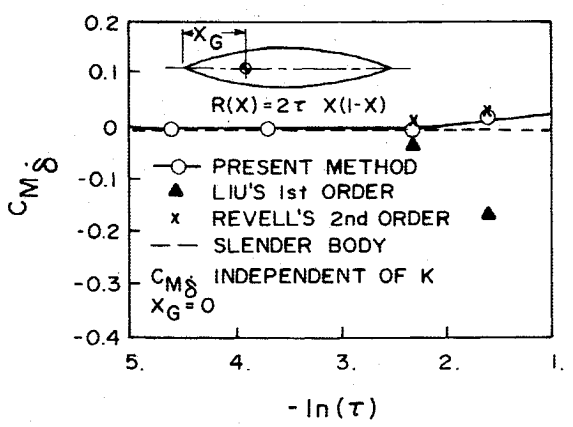


Fig. 9 Effect of thickness ratio on damping-in-pitch moment coefficient for a parabolic spindle.

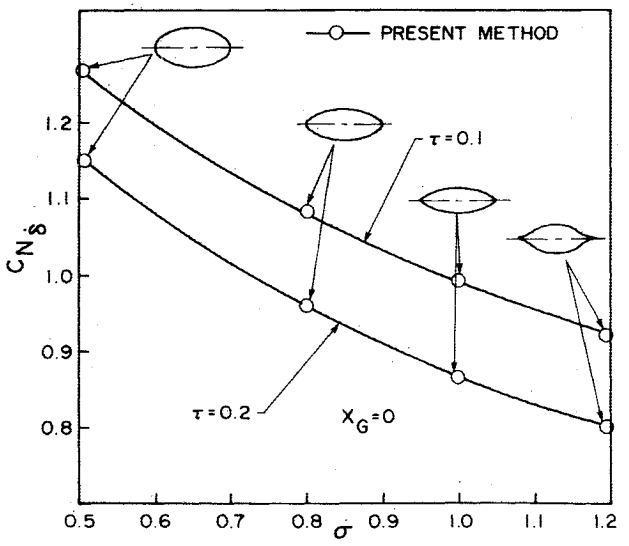


Fig. 10 Effect of nose curvature on damping-in-pitch normal force coefficient.

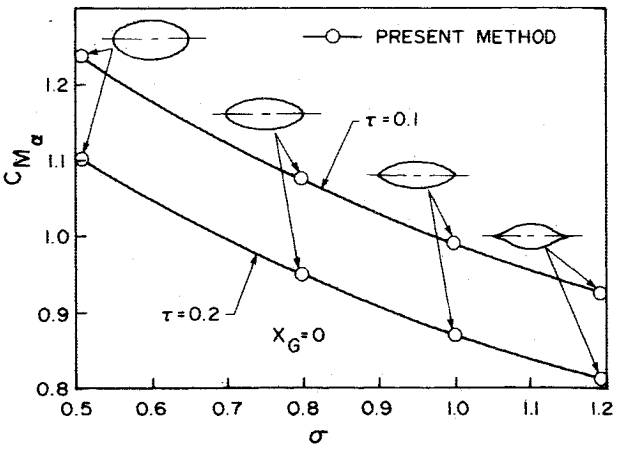


Fig. 11 Effect of nose curvature on pitching moment coefficient.

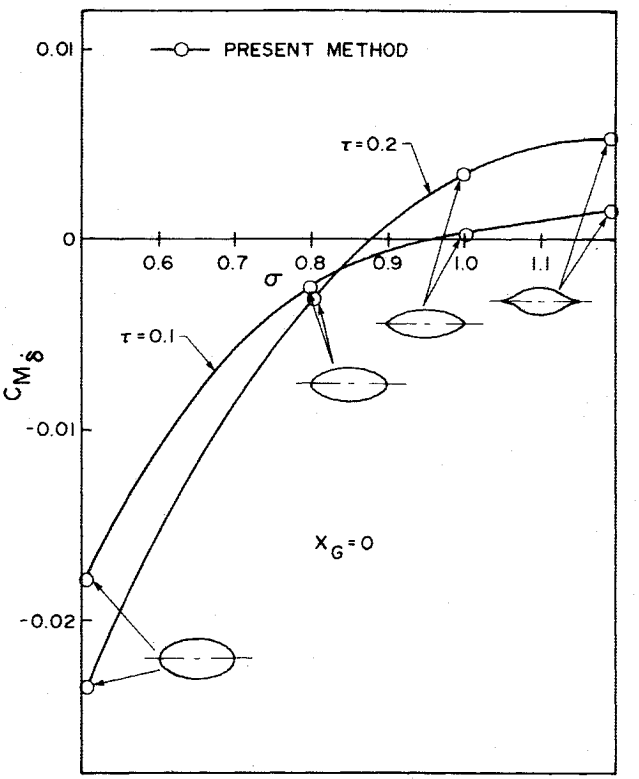


Fig. 12 Effect of nose curvature on damping-in-pitch moment coefficient.

### Bending Oscillations

Figures 13 and 14 show the effect of thickness ratio on the in-phase and the out-of-phase normal force distributions for a parabolic spindle performing first-bending oscillations. Here it can be observed that the present method contains the slender-body theory as a special case when $\tau$ decreases.

Next, Figs. 15 and 16 present the in-phase and out-of-phase pressure coefficients for an oscillating parabolic spindle in the first and second bending modes. Since the unsteady flow undergoes a more rapid acceleration (or deceleration) with the increasing order of the mode shape, the magnitude of the unsteady pressure also increases. Thus, one probably could interpret the observation that these resulting unsteady pressure distributions are left with traces of the corresponding mode shapes. It should be remarked that similar observations are noted in the cases obtained for bodies in bending oscillations in supersonic flow,[15] where larger deviations in phase angles are found as a result of strong compressibility effects.

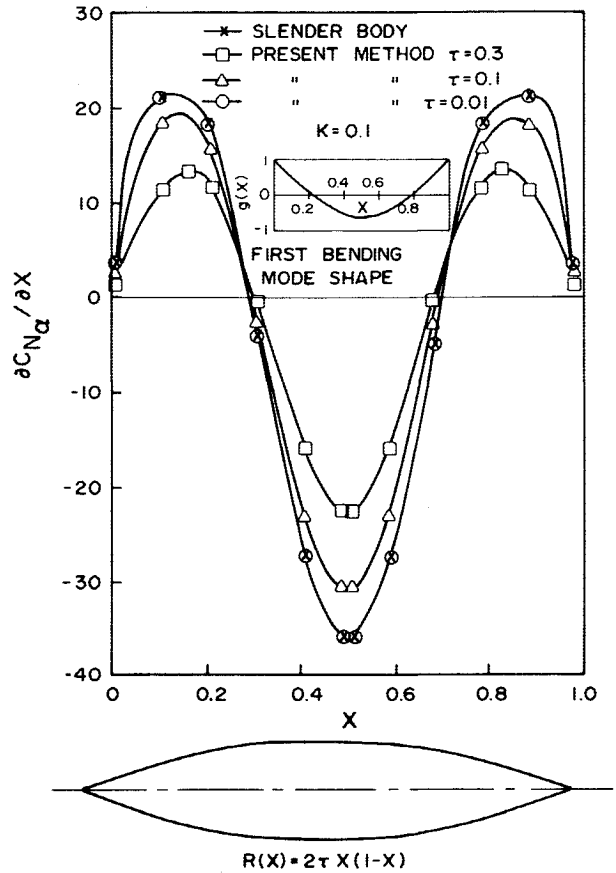


Fig. 13 Effect of thickness ratio on the local normal force coefficient for a parabolic spindle in first bending mode at reduced frequency $k = 0.1$.

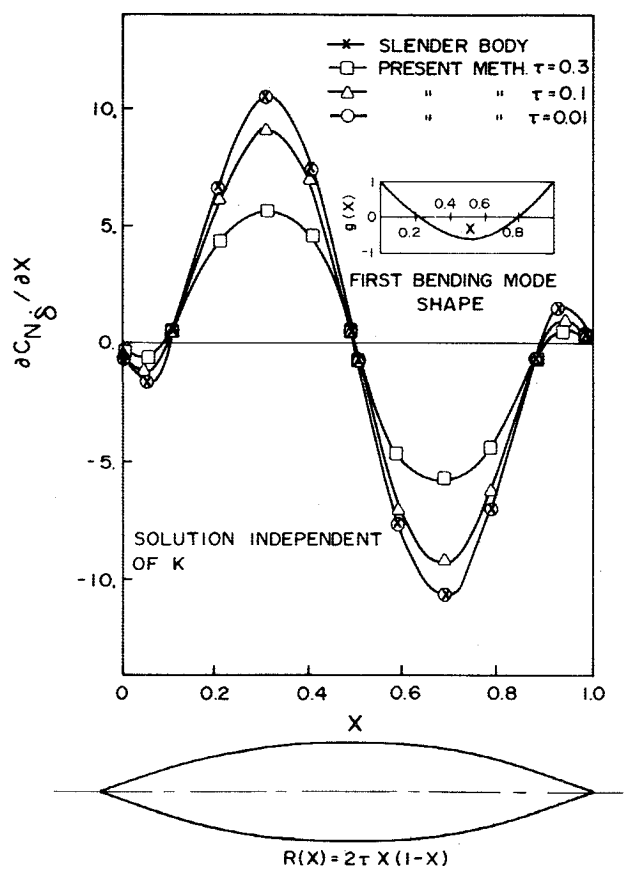


Fig. 14 Effect of thickness ratio on the local damping normal force coefficient for a parabolic spindle in first bending mode at reduced frequency $k = 0.1$.

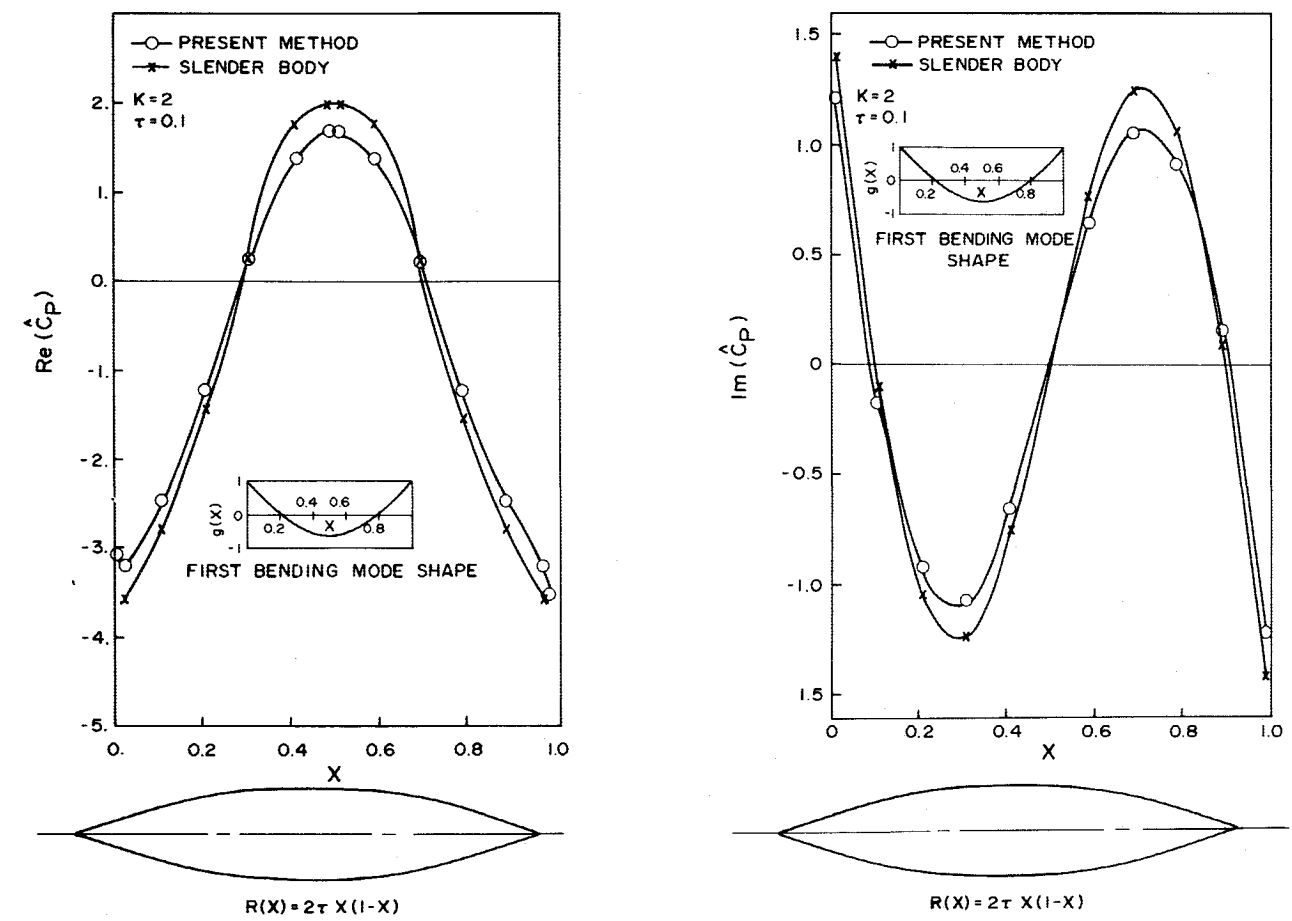


Fig. 15 In-phase and out-of-phase pressure distributions for a parabolic spindle in first bending mode at reduced frequency $k = 2.0$.

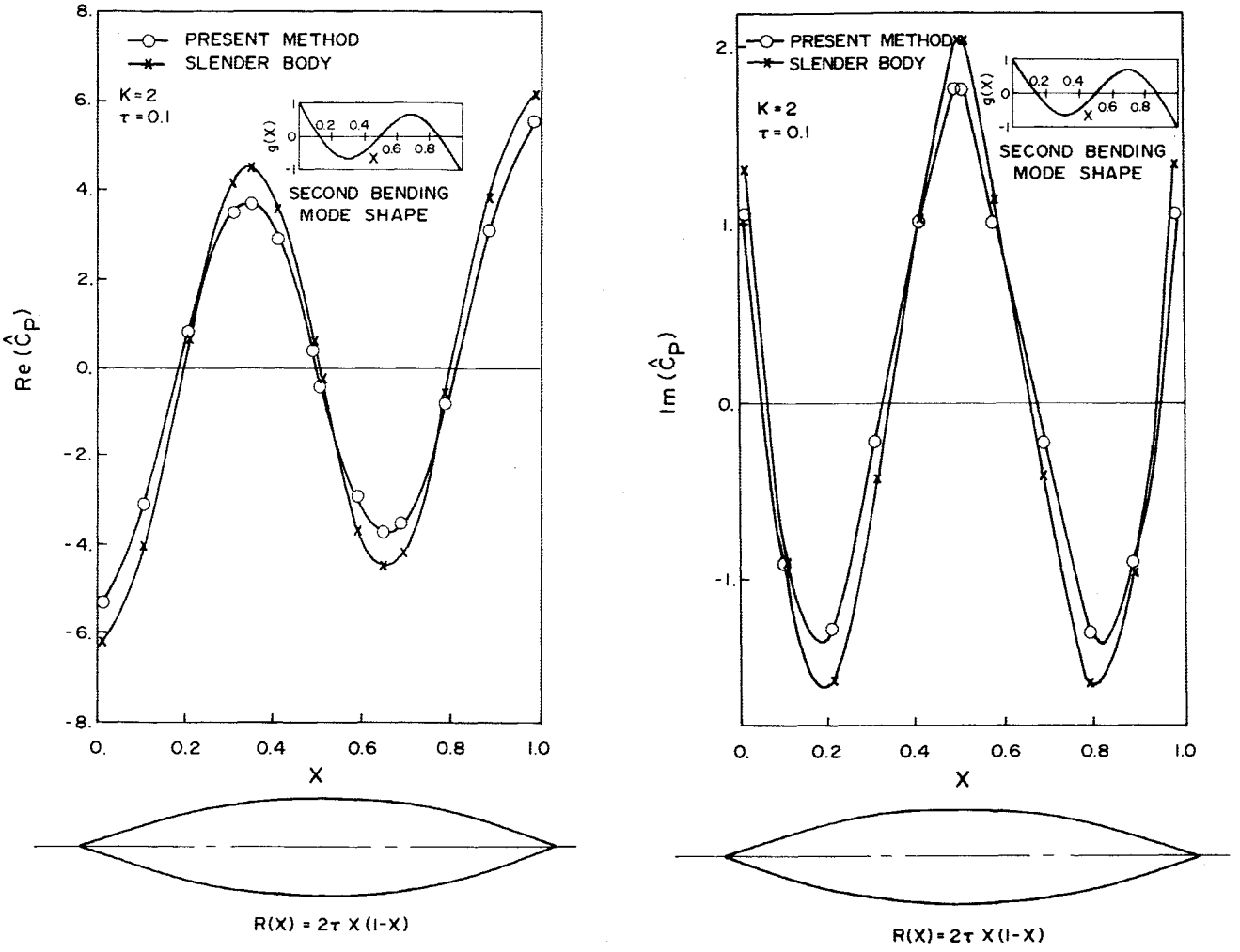


**Fig. 16 In-phase and out-of-phase pressure distributions for a parabolic spindle in second bending mode at reduced frequency $k = 2.0$.**

**Element Segmentation**

In application of the $\mu - \sigma$ rule, elements are extended all the way to the leading and the trailing edges of the body under consideration. Usually, by a cosine law of distribution, clustered segments are required near the blunted edges, while regularly spaced segments are used near the sharp edges. This is so arranged for both axial and crossflow cases, except that in the former cases, the clustered segments are retreated from the inset distance. A convergence study has been performed to establish the number of segments required for a prescribed accuracy. In terms of the force and moment calculations, it has been consistently found that 150 elements are sufficient for all results to converge to those obtained with 300 elements. To be sure, a total of 250 elements are used for all cases presented.

## Conclusions

A line source/doublet element method has been developed for computation of steady and unsteady pressures and forces and moments of an oscillating axisymmetric body in an incompressible flow. The method is effective in handling axisymmetric bodies, rigid or elastic, with smooth curvature and closed ends.

A new "$\mu - \sigma$ rule" has been derived to relate the dipole strength of the unsteady flow to the local body geometry at the apex. Such a rule can be generalized to treat bodies with convex and concave corners in compressible flows.

For steady mean flow computations, the present results are found to agree well with those of Revell's second-order method and Hess and Smith's surface-panel method. Good agreement also is found with Lamb's exact solution for inclined ellipsoids.

For rigid bodies in pitching oscillation, extensive studies on the influence of body thickness and nose bluntness on unsteady pressures and stability derivatives have been carried out. These effects can be summarized as follows:

1) On the body thickness $\tau$: statically, an increase in thickness will stabilize all the bodies, but dynamically it will destabilize bodies with sharp noses and nearly sharp (slightly blunt) noses and will stabilize blunt bodies with small nose curvatures.

2) On the nose curvature $\sigma$: an increase in the nose bluntness (i.e., a decrease in $\sigma$) tends to destabilize the body statically but stabilize it dynamically.

For the problem formulation of flexible bodies performing bending oscillations, it is simpler to introduce the wind-fixed coordinate system. Unsteady pressures are presented for a flexible body performing oscillations in the first and the second bending modes. In contrast to all previous approaches, the present results account for complete thickness and full frequency effects.

When the thickness parameter is reduced gradually, the present results approach the slender-body limit in a consistent manner for all cases. According to our studies, the results from the surface-source panel method, e.g., the USSAERO code, failed to approach such a limit.

For extensions of the present work, we recommend further development of the unsteady line source/doublet element

method for wing-body combinations, including the wake and its generalization to unsteady subsonic flows. Furthermore, the present approach can be recast into a time-domain one, which could account for arbitrary body motions.

### Acknowledgment

The authors wish to acknowledge the Army Research Office for providing them partial support. They would like to thank one of the reviewers and the Associate Editor for their constructive comments on this work.

### References

[1]Munk, M. M., "The Aerodynamic Forces on Airship Hulls," NACA Rept. 184, 1924.

[2]Laitone, E. V., "The Subsonic Flow About a Body of Revolution," *Quarterly of Applied Mathematics,* Vol. 5, No. 2, 1947, pp. 227-234.

[3]von Kármán, T., "Calculation of Pressure Distributions on Airship Hulls," NACA TM 574, 1930.

[4]Oberkampf, W. L. and Watson, L. E., "Incompressible Potential Flow for Arbitrary Bodies of Revolution," *AIAA Journal,* Vol. 12, March 1974, p. 409.

[5]Zedan, M. F. and Dalton, C., "Higher-Order Axial Singularity Distributions for Potential Flow About Bodies of Revolution," *Computer Methods in Applied Mechanics and Engineering,* Vol. 21, No. 2, 1980, pp. 295-314.

[6]Kuhlman, J. M. and Shu, J.-Y., "Potential Flow Past Arbitrary Bodies at Angle of Attack," *Journal of Aircraft,* Vol. 21, March 1984, pp. 218-220.

[7]Hess, J. L. and Smith, A. M. O., "Calculation of Potential Flow About Arbitrary Bodies," *Progress in Aeronautical Science,* Vol. 8, Pergamon, New York, 1967, pp. 1-138.

[8]Woodward, F. A., "An Improved Method for the Aerodynamic Analysis of Wing-Body-Tail Configuration in Subsonic and Supersonic Flow," NASA CR-2228, 1973.

[9]Revell, J. D., "Second Order Theory for Unsteady Supersonic Flow Past Slender, Pointed Bodies of Revolution," *Journal of the Aerospace Sciences,* Vol. 27, Oct. 1960, pp. 730-740.

[10]Revell, J. D., "Second-Order Theory for Steady or Unsteady Subsonic Flow Past Slender Lifting Bodies of Finite Thickness," *AIAA Journal,* Vol. 7, June 1969, pp. 1070-1078.

[11]Pichard, E., "Sur un Theoreme general relatif aux equation integrales de premiere espece et sur quelques problemes de physique Mathematique," *Rend Circ. mat. Palermo,* Vol. 29, 1910, pp. 79-97.

[12]Landweber, L., "An Iteration Formula for Fredholm Integral Equations of the First Kind," *American Journal of Mathematics,* Vol. 73, July 1951, pp. 615-624.

[13]Jones, R. T., "Properties of Low-Aspect-Ratio Pointed Wings at Speeds Below and Above the Speed of Sound," NACA Rept. 835, 1946.

[14]Adams, M. C. and Sears, W. R., "Slender-Body Theory-Review and Extension," *Journal of the Aeronautical Sciences,* Vol. 20, No. 2, 1953, pp. 85-98.

[15]Garcia-Fogeda, P. and Liu, D. D., "A Harmonic Potential Panel Method for Flexible Bodies in Unsteady Supersonic Flow," *Journal of Aircraft,* Vol. 24, Dec. 1987, pp. 833-840.

[16]Hoffman, G. and Platzer, M. F., "On Supersonic Flow Past Oscillating Bodies of Revolution," *AIAA Journal,* Vol. 4, Feb. 1966, pp. 370-371.

[17]Maruhn, K., "Druckverteilungreschnungen an elliptischen Rumpfen und in ihrem Aussenraum," *Jb. Lufo,* Vol. 1, 1941, pp. 135-147; Vol. 1, 1942, pp. 263-279; see also NACA Rept. 210, 1925, and NACA Rept. 323, 1929.

[18]Moran, J. P., "Line Source Distributions and Slender-Body Theory," *Journal of Fluid Mechanics,* Vol. 17, Pt. 2, 1963, pp. 285-304.

[19]van Dyke, M. D., "Second Order Slender-body Theory—Axisymmetric Flow," NASA Rept. R47, 1959.

[20]Lamb, H., *Hydrodynamics,* 6th ed., Dover, New York, 1932, pp. 139-156.

[21]Liu, D. D., Platzer, M. F., and Ruo, S. Y., "Stability Derivatives for Bodies of Revolution at Subsonic Speed," *AIAA Journal,* Vol. 14, Feb. 1976, pp. 247-250.